Contents lists available at *Dergipark*

Journal of Scientific Reports-A

journal homepage: *https://dergipark.org.tr/tr/pub/jsr-a*

E-ISSN: 2687-6167 ***Number 58, September 2024***

RESEARCH ARTICLE

Receive Date: 22.02.2024 *Accepted Date: 10.05.2024*

Thoughts of the February 20, 2023 Defne aftershock

Hatice Durmuş[a]*

[a]*Kütahya Dumlupınar University, Engineering Faculty, Department of Geological Engineering, Kütahya. ORCID: 0000-0003-4337-7302*

Abstract

On February 6 2023, two large earthquakes with magnitudes of Mw 7.8 (Pazarcık) and Mw 7.6 (Elbistan) occurred consecutively along the East Anatolian Fault Zone in eastern Turkey, causing enormous casualties and heavy damage. This devastating sequence of earthquakes was followed by the Defne aftershock on February 20 near Antakya province, which increased the damage and loss of life. In this study, the teleseismic broadband P velocity waveforms have been inverted in order to obtain the coseismic finite-fault slip distribution of the February 20, 2023 Defne aftershock. It was found that the rupture was controlled by the failure of a single asperity with the largest displacement of approximately 0.75 m, which occurred between 6 and 20 km depth. The source mechanism indicated a dominant left-lateral faulting with a significant normal component and released a total seismic moment of 5.85×10^{18} Nt.m. Coseismic Coulomb stress changes modelling showed that the Defne aftershock rupture was triggered by the earthquake sequence and that the February 6 Pazarcık earthquake had a dominant effect. In the stress modelling carried out on the Dead Sea Fault, the northern segment of the fault remained in the region of significant positive stress loading. Considering the positive stress load over 1 bar created by the earthquake sequence and the Defne aftershock ruptures, as well as the fact that no major earthquake has occurred for more than 600 years, it is clear that the probability of rupture in the northern part has increased significantly and the seismic hazard is high.

Keywords: February 20, 2023 Defne aftershock; finite-fault inversion; Coulomb stress changes; Dead Sea Fault

1. Introduction

On 6 February 2023, two devastating earthquakes struck south-central Turkey and ruptured the southwestern part of the East Anatolian Fault Zone (EAFZ). The first earthquake was the Mw 7.8 Pazarcık earthquake (at 4:17 am

* Corresponding author:
E-mail address: hatice.durmus@dpu.edu.tr

GMT), followed by the Mw 7.6 Elbistan earthquake (at 10:24 pm GMT) (Fig. 1). These earthquakes were the largest since the 1939 Erzincan earthquake and were felt across a large part of Turkey, resulting in widespread destruction, loss of life, and economic damage. The earthquakes affected about 450 kilometres from Adana in the west to Diyarbakır in the east and 300 kilometres from Malatya in the north to Syria in the south. It affected eleven provinces, including Kahramanmaraş, Adana, Hatay, Gaziantep, Adıyaman, Diyarbakır, Malatya, Şanlıurfa, Kilis, Osmaniye, and Elazığ, where approximately 13.5 million people reside [1]. In the report published by the Presidency Strategy and Budget of the Republic of Türkiye, it was stated that more than 48 thousand people lost their lives, and more than half a million buildings were destroyed or severely damaged as a result of the earthquakes [2]. According to the World Health Organization's July 2023 report, more than 50,000 people lost their lives, 45.968 in Turkey and 5.900 in Syria, more than 107,000 people were injured, and 3 million people had to leave their homes [3].

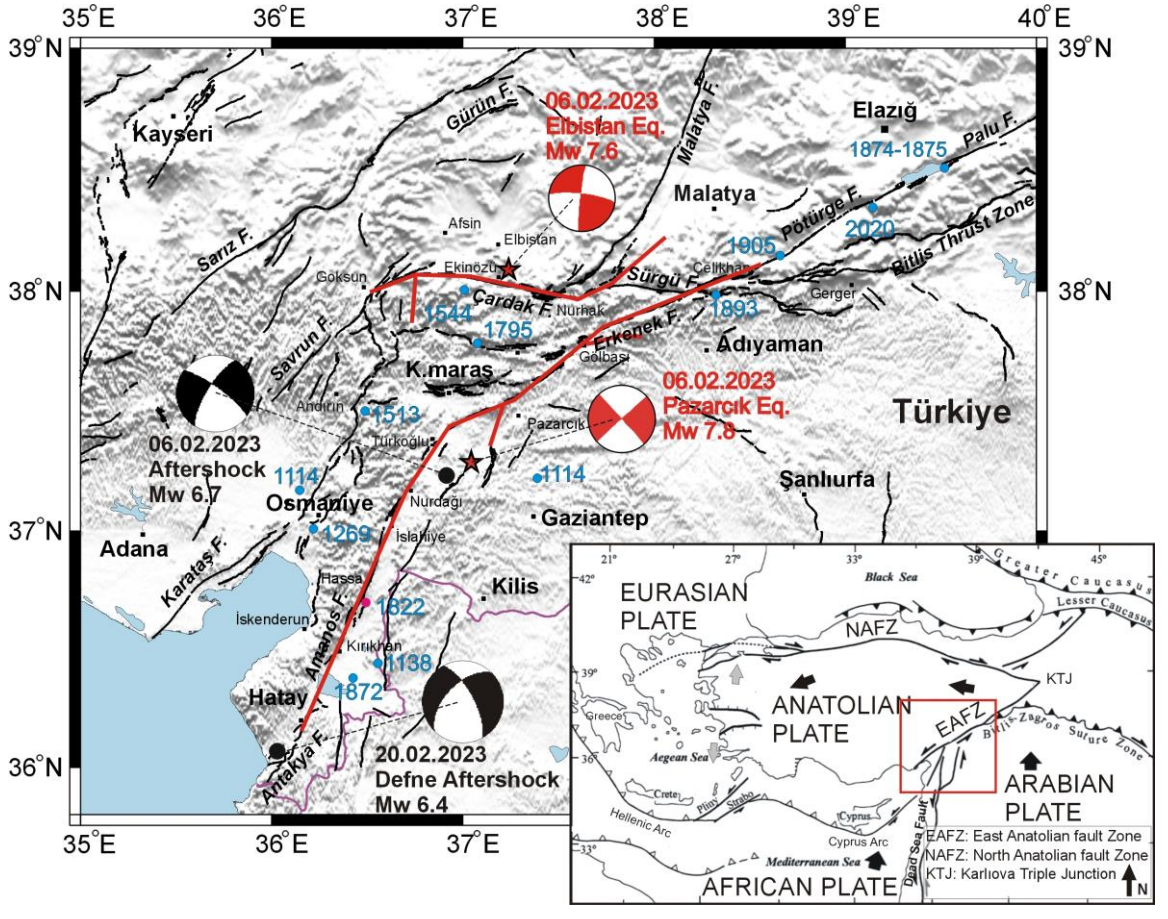

Fig. 1. Major tectonic elements of Turkey (inset) and the seismotectonic of eastern Turkey. Large arrows in the inset map indicate the direction of relative plate motions. The earthquake source mechanisms and epicentres are taken from the catalogue of the Disaster and Emergency Management Authority (AFAD). The active faults are compiled from [4] and [5]. Red lines are surface ruptures of February 6, Pazarcık and Elbistan earthquakes taken from [6]. The map's information was collated from [6-14].

Turkey's main tectonic structures result from the movement between the Arabian, African, Eurasian, and Anatolian plates. In the east, the Arabian Plate converges towards the Anatolian Plate in the northwest direction at a rate 18 mm/year [15, 16] (Fig. 1 inset map). With this convergent movement, the Anatolia was compressed and thickened, and after the compression reached a level that the continental crust could not bear, the Anatolian plate moved westward along two important strike-slip fault systems. [7, 17-19]. The fault systems under consideration are, respectively, the North Anatolian Fault Zone (NAFZ), which exhibits a right lateral strike-slip motion and the East Anatolian Fault Zone (EAFZ), which displays a left lateral strike-slip motion. (Fig.1 inset map). The NAFZ, 1.200 km long, extends from the Karlıova triple junction (KTJ), intersecting with the EAF in the Karlıova region, to the Marmara Sea [20-24] and has a slip rate of approximately 24 mm/year [15, 16, 25]. The EAFZ, on the other hand, extends for about 580 km from the KTJ to the Dead Sea fault in the southwest (Fig. 1). It also has a Northern Branch, which branches off the main fault immediately west of Çelikhan and extends through the Adana Basin to the Mediterranean Sea. (Figs. 1) [5, 24, 26, 27]. GPS studies indicate a slip rate of 9-10 mm/yr for the EAFZ [15, 16, 25], of which about one third is contributed by the Northern Branch after the bifurcation. [10, 26, 28, 29]. Based on data from field studies, a geological slip rate of about 8 mm/yr has also been proposed. [5, 30].

In the 20th and 21st centuries, the NAF was ruptured in a series of earthquakes, beginning with the 1939 Erzincan earthquake and continuing with the 1999 Mw7.9 Izmit and Mw7.2 Düzce earthquakes, which extended as far as the Gulf of Izmit in western Turkey [20, 31, 32]. The historical and instrumental records show that this region has been affected by devastating earthquakes for almost 2,000 years. [20, 33-36]. Significant earthquakes that occurred in the historical period on the segments forming the EAFZ were respectively 29 November 1114 (M> 7.8), 28 March 1513 (M > 7.4), 1822 Antakya Earthquake (M_S= 7.5), 1866 Karlıova-Bingöl Earthquake (M_S = 7.2), 1872 earthquake (M_S = 7.2), 1874 (M_S = 7.1) and 1875 (M_S = 6.7) earthquakes and 2 March 1893 Malatya Earthquake (M_S = 7.1) [37] (Fig. 1). Compared to its activities in the 19th century, the EAFZ was relatively quiet in the 20th century [8, 37]. In the 20th century, the only earthquakes along the EAFZ were the 1905 Malatya and 1971 Bingöl earthquakes. The recent occurrence of the 2003 Bingöl, 2010 Başyurt and 2020 Sivrice-Doğanyol earthquakes and the current occurrence of the 2023 Pazarcık (Mw=7.8) and Elbistan (Mw=7.6) earthquakes suggest that the fault is much more active in the 21st century [14, 39, 40]. Historical earthquakes [8] and Coulomb stress change modelling [38, 41-43] along the EAFZ indicate that the fault segment between Gölbaşı and Türkoğlu creates a seismic gap. At the same time, paleoseismological studies have revealed the existence of a high seismic hazard risk along the southwestern part of the EAFZ after hundreds of years of silence [44]. The data from the trenches that have been dug along the fault indicate that the earthquakes of 1114 and 1513 were the most recent earthquakes to rupture the gap [45]. The 6 February Maraş earthquakes occurred in this seismic gap, which has remained silent for more than 500 years, and the 1114, 1513, 1544 earthquake ruptures and a part of the 1893 earthquake rupture broke again.

Due to the earthquakes, many aftershocks occurred in the region. One of these is the largest aftershock with a magnitude of Mw=6.7, which occurred southwest of the Pazarcık earthquake epicentre, immediately after the 6 February Pazarcık earthquake (Fig. 1). The other is the Defne aftershock with an instrumental magnitude of Mw=6.4, which occurred on February 20, 2023, around Yayladağı (Hatay) at 20.04 local time, two weeks after the February 6 earthquakes. The epicenter of the Defne aftershock is situated on the Antakya Fault Zone [46], a dip-slip normal fault characterised by a left-lateral strike-slip component. This fault zone extends approximately 45 km in length (Fig. 1). Due to this aftershock, 6 people died and 294 people were injured, 18 of them seriously [47]. The hypocentral and source parameters of these earthquakes estimated by different seismological organizations and previous studies given Table 1.

Earthquake sequences that result in large-magnitude events separated by short-time intervals can cause great loss of life and destruction (for example, the 2019 Ridgecrest earthquakes, the 2022 Iran earthquake sequence and the 2022 Taiwan earthquakes). In addition, major aftershocks that occur after the main shock can increase the damage caused by the main shock and cause even greater loss of life and destruction. An example of this is the February 22, 2011 Christchurch earthquake. While no loss of life was observed during the 2011 Christchurch mainshock, 182 deaths occurred due to the devastation that occurred after the aftershock, as the aftershock hypocenter was located

shallower and right under the town of Christchurch [51]. Another example in this context is the November 9, 2011 Edremit aftershock (Mw = 5.7), which occurred after the October 23, 2011 Van earthquake (Mw=7.1) [52, 53]. Although there was relatively little destruction and loss of life in the city centre of Van during the main shock in the 2011 Van earthquake series, the Edremit aftershock particularly affected the city of Van, causing additional destruction and loss of life. The most recent and striking example is the February 6 Pazarcık and Elbistan earthquakes, which occurred in our country. While the occurrence of two major devastating earthquakes 9 hours apart caused great loss of life and damage in a wide area covering 11 provinces, the loss of life and damage increased even more, especially in Hatay province, with the Defne aftershock that occurred two weeks later on February 20. In this context, the fact that two earthquakes occurred within 9 hours and were followed by the Defne aftershock two weeks later makes it valuable to reveal the triggering relationship between these three earthquakes.

It has been suggested that changes in the Coulomb failure stress occur in such a way as to trigger earthquakes [54, 55]. In the past, many crucial studies have been conducted showing that positive Coulomb failure stress plays a role in bringing the fault closer to failure and, therefore, earthquake occurrence, while negative Coulomb failure stress plays a role in delaying subsequent earthquakes [56-68]. In addition, aftershock distribution characteristics can be determined by modelling Coulomb stress changes after the main shock [60, 65, 69-72]. In this context, calculations of the change in Coulomb stress are of great importance for understanding the time-dependent interactions between earthquakes and assessing seismic hazards. In this study, the spatial distribution of the coseismic finite fault rupture of the February 20, 2023, Defne earthquake was obtained, and the triggering effect of the February 6 earthquake sequence (the February 6 Pazarcık earthquake, the largest aftershock and the February 6 Elbistan earthquake) on the rupture of the Defne earthquake was revealed.

Table 1. Various seismological organisations and previous studies have estimated hypocentral and source parameters.

	Lat (°)	**Long (°)**	**Mw**	**Strike (°) NP1/NP2**	**Dip (°) NP1/NP2**	**Rake (°) NP1/NP2**	**Depth (km)**	**Max. slip (m)**	**Seismic Moment (Nt.m)**
February 6, 2023, Pazarcık Earthquake									
USGS-NEIC	37.226	37.014	7.8	228/318	89/89	-1/-179	17,5		$5.389x10^{20}$
GCMT	37.55	37.45	7.8	51/143	70/86	-4/-160	15.1		$5.8x10^{20}$
KOERI	37.13	37.13	7.7	222/324	64/65	-27/-152	10		$3.78\ x10^{20}$
AFAD	37.288	37.043	7.7	233/140	74/77	18/168	8.6		
[46]									$6.39\ x10^{20}$
[6]			7.8	43	88	0		9.7	$5.62\ x10^{20}$
[48]			7.8					8	$5.4\ x10^{20}$
[50]			7.82					9	$7.1\ x10^{20}$
[49]			7.8					9	$6.51\ x10^{20}$
February 6, 2023, Largest Aftershock									
USGS-NEIC	37.189	36.893	6.7				9.8		
GCMT	37.21	36.84	6.8	212/306	73/78	-13/-163	26.2		$1.85\ x10^{19}$
KOERİ	37.233 7	36.7805	6.6				5		
AFAD	37.304	36.92	6.6	300/187	70/43	-128/-30	6.2		
February 6, 2023, Elbistan Earthquake									
USGS-NEIC	38.011	37.196	7.5	277/186	78/87	4/168	13.5		$2.637\ x10^{20}$
GCMT	38.08	37.22	7.7	264/0	46/83	-9/-136	12		$4.53\ x10^{20}$
KOERI	38.05	37.26	7.6	273/6	67/81	-9/-157	10		$2.73x10^{20}$
AFAD	38.089	37.239	7.6	358/90	73/86	174/13	7		
[46]									$3.23\ x10^{20}$
[6]			7.7	261	70	-4		8.1	$4.53\ x10^{20}$
[48]								5	$3.3\ x10^{20}$
[50]			7.7	282	70	0		10	$5.0\ x10^{20}$
[49]			7.6					7	$3.64\ x10^{20}$
February 20, 2023, Defne Aftershock									
USGS-NEIC	36.162	36.025	6.3	333/225	69/53	-139/-27	11.5		$4.09\ x10^{18}$
GCMT	36.06	36.03	6.3	226/328	42/79	-16/-131	12		$4.08\ x10^{18}$

KOERI	36.10	36.13	6.4	330/225	68/56	-143/-25	16		3.63×10^{18}
AFAD	36.037	36.021	6.4	214/332	57/55	-44/-138	21.73		
[48]			6.4	237	55	12		0.93	
[6]				231	47.5	-0.2		1	
This study				225	53	-27	13.4	0.75	5.85×10^{18}

USGS-NEIC: United States Geological Survey-National Earthquake Information Center; GCMT: Global Centroid Moment Tensor Project; KOERI: Kandilli Observatory and Earthquake Research Institute; AFAD: Republic of Turkey Ministry of Interior Disaster and Emergency Management Authority

2. Finite-fault inversion, model parametrization and results

For the finite-fault analysis of the February 20 Defne aftershock, 21 teleseismic broadband displacement P waveforms recorded by the Global Digital Seismograph Network (GDSN) and obtained from the Incorporated Research Institutions for Seismology (IRIS) were used. The slip distribution model was obtained via the linear finite-fault inversion method, a technique that has been employed for several decades to determine rupture characteristics of earthquakes (see references [73-79] for more detail). In applying the method, a two-dimensional model fault plane is first defined to represent the source of the earthquake (fault length and fault width). This is followed by the division of the model fault plane into subfaults, which enables the spatial distribution of slip to be determined. Accordingly, for the rupture of the Defne aftershock, a single-segment rectangular fault plane of 50 x 25 km^2 was selected and divided into 50 square subfaults (Fig. 2a, along strike 10, along down dip 5). The strike, dip and rake angle of the initial model fault plane were taken as 225°, 53° and -27°, respectively, by considering the source mechanism solutions given in Table 1 and placed within the crustal velocity field. The hypocenter location (36.110°N, 26.062°E) and hypocenter depth (13.4 km) given by the USGS were taken as the starting point of the rupture, and many inversion attempts were made. To simulate rupture front propagation along the model fault plane, 25-point sources were uniformly distributed on each subfaults and point source responses were calculated by applying Generalized Ray Theory [80]. The elastic responses obtained in this way were summed with the appropriate time delay, and artificial seismograms were calculated for each station (Fig. 2b).

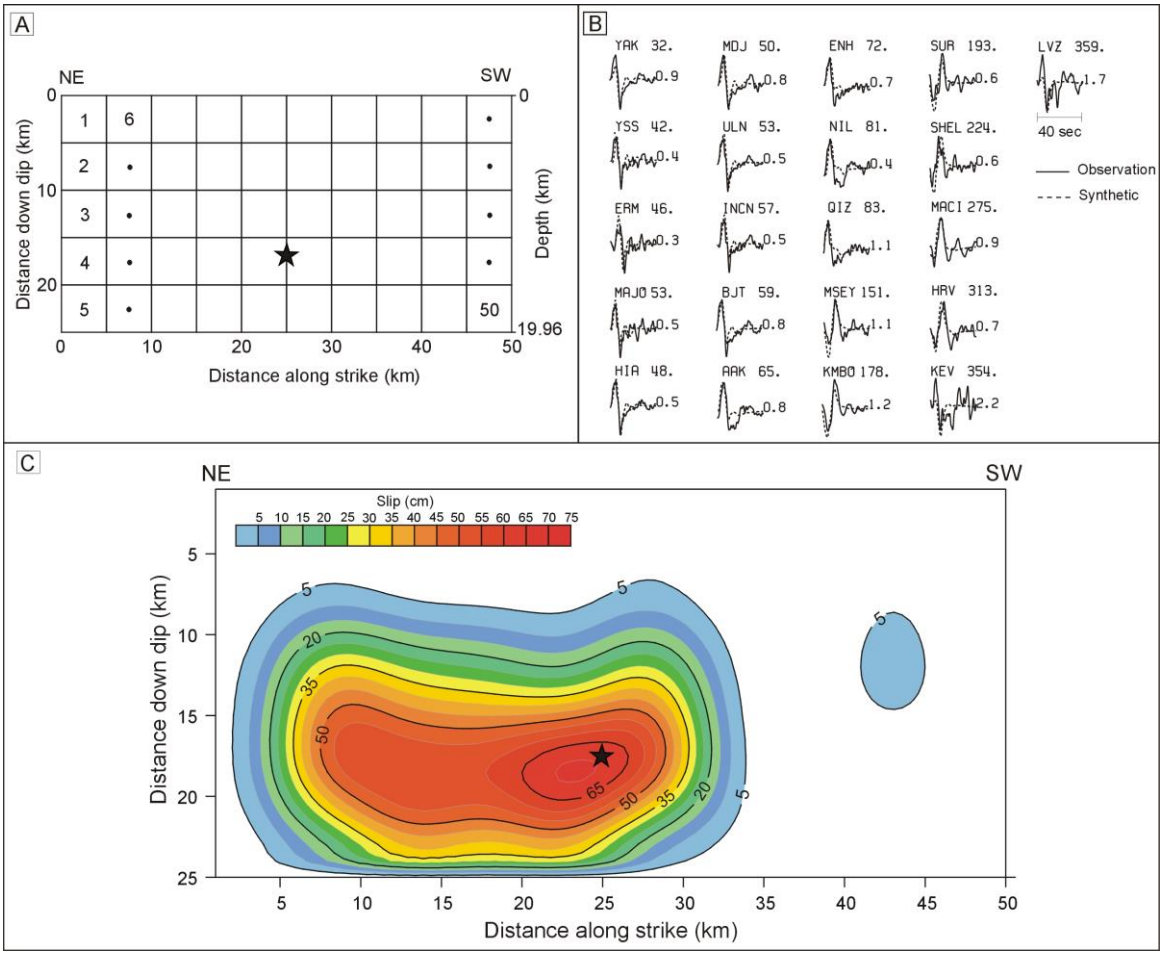

Fig. 2. (a) Defne aftershock model fault plane parameterizations used in the study; (b) comparison of the predicted P and SH waveforms calculated for the slip model and (c) preferred co-seismic slip distribution obtained from the finite-fault analysis. The slips are contoured at 5 cm intervals and only slips that are greater than 5 cm have a contoured. Solid stars represent the hypocenters.

Comparison of observed waveforms and fault segment synthetic waveforms Ax≅b the system of linear equations is over-defined. Here, matrix A is the matrix of fault segment synthetic seismograms, and b is the matrix of observed seismograms at each station combined. x is the solution matrix containing the slip weights to be assigned to each fault segment to ensure the agreement between the synthetic and the observed seismograms, and the Householder least squares inversion method was used for its calculation. Six-time windows were used in the inversion, and the source rise-time function within each time window was represented by an equilateral triangle with a rise and fall of 0.4 s, allowing a total rise time of 4.8 s at each point on the fault plane. Using this time window approach to modeling allows for variations in rupture velocity and slip rise time on the model fault plane, allowing for accurate modeling of complex source properties. The initial rupture velocity for the inversion was taken as 3.0 km/s ([81] emphasized that the rupture velocity varies between 70% and 90% of the S-wave velocity for many earthquakes), but inversions were also attempted for different rupture velocities. A detailed description of the method is given by [73] and [76].

In order to obtain the best fitting slip distribution model to the data, a large number of inversion experiments were performed for different source parameters and different values of rupture velocity and focal depth. Accordingly, the model with a rupture velocity of 3.3 km/s, a focal depth of 13.4 km, and strike, dip, and rake angles of 225°, 53° and -27°, respectively, gave the best fit to the data. A comparison of the observed and synthetic waveforms and the slip distribution pattern of the resulting model are given in Figs. 2b and c, respectively. The unconformity between observed and synthetic waveforms for different inversion trials is defined as the L2 Euclidian norm (‖b-Ax‖) [82].

The finite-fault slip distribution model of the Defne aftershock indicates that the rupture was caused by the failure of a single fault asperity. Covering an area of 35 km x 18 km between depths of 6 and 20 km, the largest slip reached 0.75 m near the hypocenter. The rupture was confined at the hypocenter and proceeded unilaterally towards the northeast. It released a total seismic moment of 5.85×10^{18} Nt.m (Mw=6.4).

3. Coulomb stress changes modeling

When earthquakes occur, they cause a change in the stress state on the neighbouring faults around them, and in this way, they can trigger an earthquake that will occur around the mainshock, bringing it forward or delaying it [57, 60 83-68]. Many studies have shown that there is a stress-triggering relationship between medium and large earthquake sequences (etc. 1999 İzmit (Mw7.4) and Düzce (Mw7.2) earthquake sequence [79]; 2015 Nepal (Mw7.8) and Mw7.1 earthquake sequence [89]; 2019 Ridgecrest (M6.4) and Mw7.1 earthquake sequence [90-92]) and that there is a relationship between successive mainshock-aftershock occurrences and earthquake stress changes [61, 63, 64, 72].

Coulomb failure criteria are widely used to characterize the conditions under which failure occurs and;

$$\Delta\sigma_f = \Delta\tau + \mu'\Delta\sigma_n \quad (1)$$

is expressed by the relation. Here, $\Delta\tau$ and $\Delta\sigma_n$ changes in shear stress and normal stress on the target fault plane, μ' is the effective friction coefficient, including the unknown effects of pore water pressure [60, 63]. It is emphasized that μ' is a value ranging between 0.2-0.8 and has no critical effect on Coulomb stress calculations, and taking it as 0.4 reduces the margin of error in modeling results by 25% [60, 61, 97, 98]. Accordingly, μ' value was taken as 0.4, Young's modulus as 8×10^5 bar and Poisson's ratio as 0.25 in all stress calculations performed within the scope of the study. Stress changes were calculated using [99]'s coseismic elastic dislocation model by considering earthquake ruptures as rectangular dislocation surfaces in an elastic semi-infinite medium. A Coulomb stress change value greater than zero (positive) indicates that fracture has become probable, while a negative value indicates the opposite. The Coulomb 3.2 package program was used for the calculations [68, 100], and the increase in stress is represented in red and the decrease in blue.

The focal and source parameters (strike, dip, rake and fault dimension) of the earthquakes that constitute the source in the coseismic coulomb stress change calculations are summarized in Table 2 (the February 6 Pazarcık, the largest aftershock, the February 6 Elbistan and the Defne aftershock). For the February 6 Pazarcık and Elbistan earthquakes, the fault slip distribution model obtained by [6] based on coseismic InSAR and GPS displacements was used. The homogeneous rupture model dimensions (fault length x fault width) and the maximum slip value for the largest aftershock were determined as 30 km x13 km and -0.90 cm, respectively (depending on the magnitude (Mw=6.7)) based on the empirical relations of [101]. Fault parameters given by GCMT were used for the determined rupture model, and this fault plane was placed in the source region.

Table 2. Source earthquake rupture parameters in Coulomb stress change modelling.

Earthquake Name	**Date**	**Lat. Lon. (º)**	***M*w**	**Strike (º)**	**Dip (º)**	**Rake (º)**	**Fault length (km)**	**Fault width (km)**	**Max Slip (m)**	**Ref.**
Source Earthquakes										
February 6 Pazarcık	06.02.2023	37.288 37.043	7.8	S1 21.1 S2 34.3 S3 66.9 S4 50.7 S5 67.7 S6 205 S7 8.3 S8 92.3	88	0	175	20.00	Variable	[6]
Largest Aftershock	06.02.2023	37.189 36.893	6.7	212*	73*	-13*	30	13	-0.90	[101] *GCMT
February 6 Elbistan	06.02.2023	38.089 37.239	7.6	S1 249.1 S2 269.4 S3 281.9 S4 245.1 S5 231.4 S6 2.3	70	-4	150	21.28	Variable	[6]
Defne Aftershock	20.02.2023	36.110 36.062	6.4	225	53	-27	35	25	Variable	This study

The map view of the Coulomb stress change models calculated to investigate whether the February 6 earthquake sequence triggered the Defne aftershock rupture is shown in Figs. 3 and 4. Stress patterns were calculated on the Defne aftershock rupture plane, from which we obtained the slip distribution model (Strike=225°, Dip=53°, Rake=-27°), and for a depth of 13.4 km corresponding to its hypocenter depth. Fig. 3a shows the stress changes calculated for the February 6 Pazarcık earthquake, Fig. 3b for the largest aftershock and Fig. 3c for the February 6 Elbistan earthquake.

Fig. 3 shows that the rupture plane of the Defne aftershock was subjected to positive stress due to the February 6 Pazarcık and the largest aftershock earthquakes and negative stress due to the February 6 Elbistan earthquake. This suggests that the February 6 Pazarcık and the largest aftershock earthquakes triggered the rupture of the Defne aftershock. In order to reveal the triggering stress effect of each earthquake, stress values were calculated at different epicentral locations (Fig. 3) and hypocentral depths given by USGS, GCMT, AFAD and KOERİ for the Defne aftershock (Table 3). The high positive Coulomb stress values calculated at all hypocentral locations revealed that the rupture of the Defne aftershock was predominantly caused by the triggering effect of the rupture of the February 6 Pazarcık earthquake.

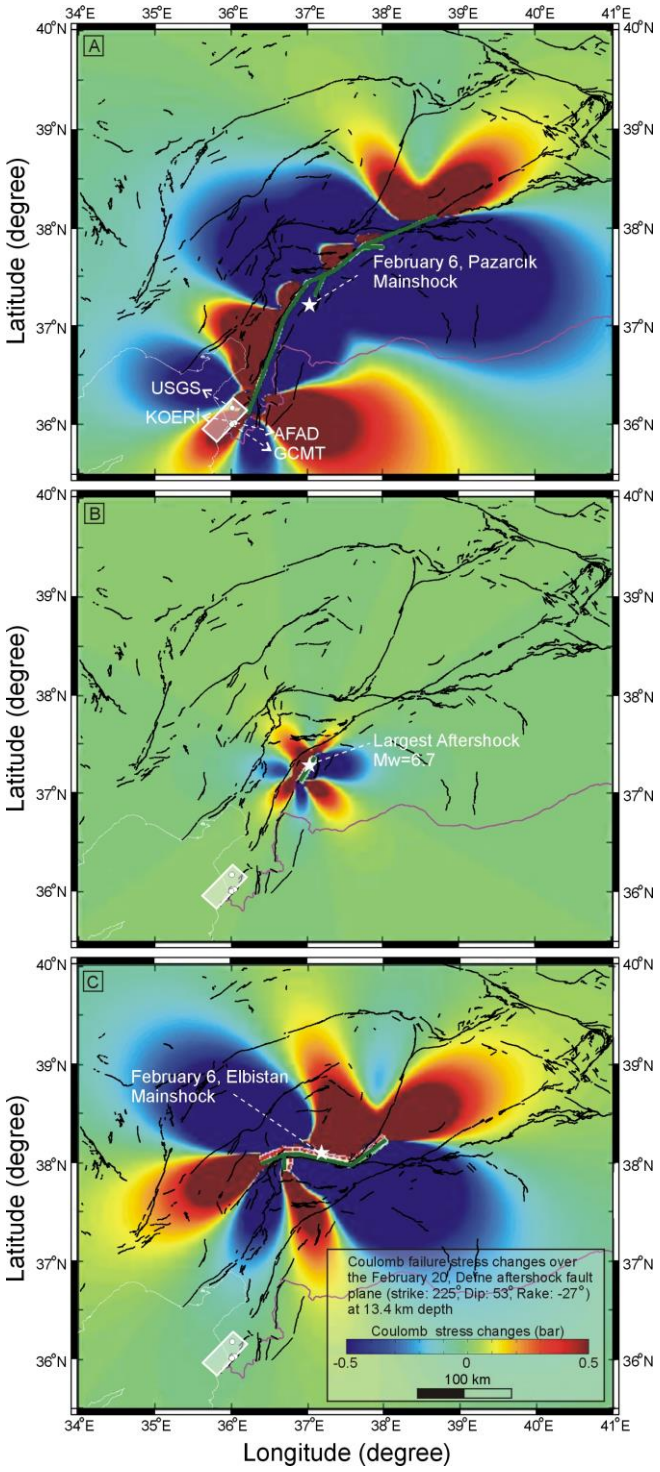
A
February 6, Pazarcık
Mainshock
USGS
KOERİ
AFAD
GCMT
B
Largest Aftershock
Mw=6.7
C
February 6, Elbistan
Mainshock
Coulomb failure stress changes over the February 20, Defne aftershock fault plane (strike: 225°, Dip: 53°, Rake: -27°) at 13.4 km depth
Coulomb stress changes (bar)
-0.5
0
0.5
100 km
Latitude (degree)
Longitude (degree)
34°E
35°E
36°E
37°E
38°E
39°E
40°E
41°E
36°N
37°N
38°N
39°N
40°N

Fig. 3. Map view of Coulomb stress change over the Defne aftershock fault plane caused by (a) the February 6 Pazarcık; (b) the largest aftershock; (c) the February 6 Elbistan earthquake. Green lines are fault planes on the surface for earthquakes. The white rectangle is the Defne aftershock fault plane. White circles indicate the location of the Defne aftershock by USGS, KOERİ, AFAD and GCMT, respectively. White stars are earthquake epicentres according to AFAD.

In order to examine the combined effects of the earthquakes, Fig. 4a shows the map image of the Coulomb stress change model calculated on the rupture plane of the Defne aftershock due to February 6 Pazarcık and the largest aftershock earthquakes. Fig. 4b shows the map image of the Coulomb stress change models calculated on the rupture plane of the Defne aftershock due to the February 6 earthquake sequence. When Figs. 4a and b are analyzed, it is noteworthy that the rupture plane of the Defne aftershock is located in the area of positive Coulomb stress increase.

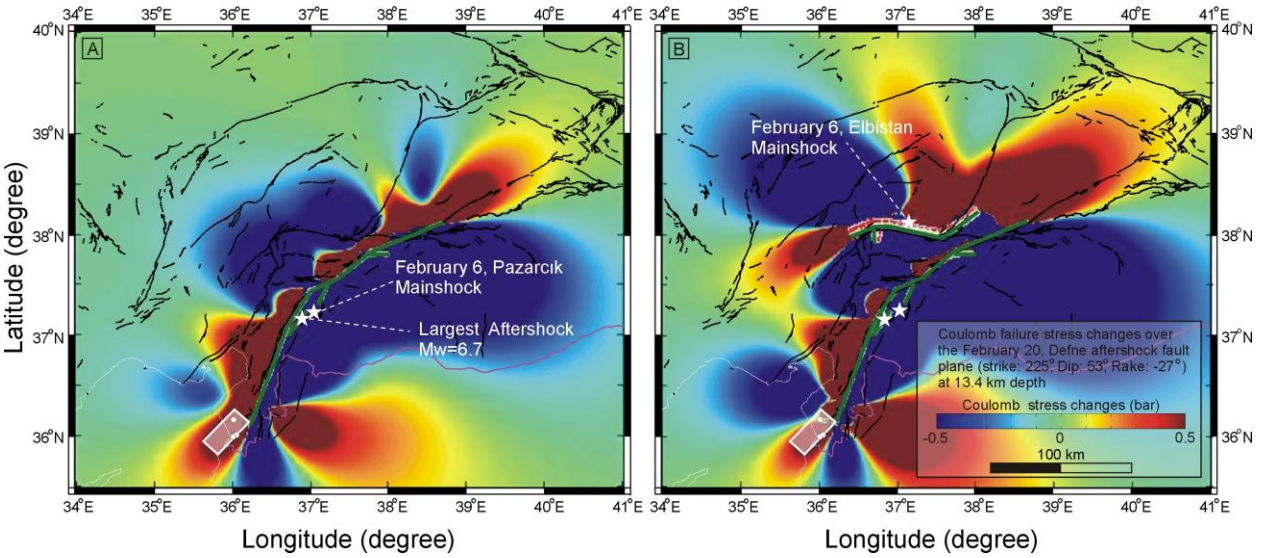

Fig. 4. The map view illustrates the change in Coulomb stress changes over the Defne aftershock fault plane resulting from (a) the February 6, Pazarcık and the largest aftershock earthquakes; (b) the earthquake sequence. See labels within the figures caption of Fig. 3 for the other details.

In order to determine the triggering relationship of earthquake ruptures on neighboring faults, Coulomb stress changes were calculated on the DSF, which extends in the N-S direction just south of the February 6, earthquake sequence and the Defne aftershock ruptures (Fig. 5). The direction of the plane where the stress changes were calculated for the DSF was determined from the map trace (180°), and the dip and rake angle were taken as 87° and 0°, respectively [102]. Calculations were made for a depth of 10 km. Firstly, the Coulomb stress change model was calculated on the DSF where the February 6 earthquake sequence and the Defne aftershock earthquakes were defined as the source fault, and it was noted that a positive stress field of over 1 bar was formed in the northern part (Fig. 5a). When the stress change model was calculated only due to the rupture of the Defne aftershock, a very low positive stress field was obtained in the same part (Fig. 5b).

Stress values were calculated at four different points (Fig. 5; P1, P2, P3 and P4) to determine the spatial distribution of stress changes along the northern part of the DSF (Table 3). Accordingly, points P1 and P2 on the western segment in the northern part of the DSF were predominantly loaded with positive stress above 1 bar due to the February 6 Pazarcık earthquake, while point P4 was loaded with positive stress around 0.5 bar. While the rupture

of the Defne aftershock created a negative stress field in the south, it had a very small positive stress loading effect on points P1 and P3 in the north (Fig. 5, Table 3).

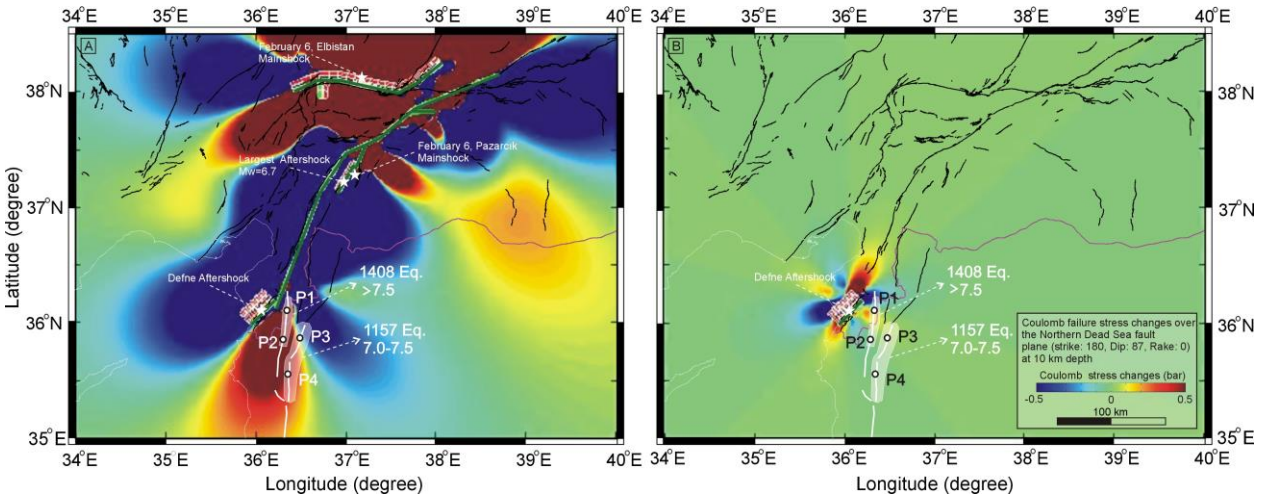

Fig. 5. Map view of Coulomb stress change over the northern part of the DSF caused by (a) February 6, earthquake sequence and the Defne aftershock earthquakes; (b) the Defne aftershock. White circles indicate the points for which the stress values are sampled (see Table 3). Fault traces of the DSF were taken from [104].

4. Discussion

In this study, the finite-fault slip distribution model of the Defne aftershock is derived from the inversion of broadband teleseismic P waveforms. The coseismic slip distribution model shown in Fig. 2c indicates that the Defne aftershock rupture occurred with a maximum slip of 0.75 m, with a single fault asperity over a fault area of 35 km by 18 km. The rupture started at the hypocenter, propagated unilaterally to the NE and released a total seismic moment of 5.85×10^{18} Nt.m. The finite-fault slip distribution model is relatively similar to the slip distribution models obtained by [6] and [48] based on InSAR data, except for the maximum amount of slip. Their slip distribution models show a slip value of about 1 meter around the hypocenter, while the finite-fault slip distribution model shows a relatively low slip value of 0.75 m. All the obtained models show that the rupture propagated to the NE and completed its maximum slip in an area including Hatay province. This explains why the loss of life and damage from the Defne aftershock was more severe in Hatay.

The Coulomb stress change maps created to investigate whether the rupture of the Defne aftershock occurred due to stress triggering revealed that the rupture of the Defne aftershock occurred in the area of positive stress loading (Fig. 3). The February 6 Pazarcık and the largest aftershock created a triggering positive stress load on the rupture plane of the Defne aftershock, while the February 6, Elbistan earthquake created a negative stress shadow. [40] and [84] emphasized that the triggering threshold for a critical fault close to failure is 0.1- 0.5 bar. Accordingly, when Table 3 is analyzed, the triggering effect of the February 6, Pazarcık earthquake on the rupture of the Defne earthquake is clearly seen (>1 bar). Positive stress values ranging from 0.002 to 0.005 bar originating from the largest aftershock indicate that this stress effect is negligible. The February 6 Elbistan earthquake created a stress shadow between -0.030- -0.040 bar at all epicenter locations given. This is interpreted as the rupture of the February 6 Elbistan earthquake with very low negative stress values did not have a delaying effect on the rupture of the Defne aftershock.

In order to reveal the combined effect of earthquake ruptures in Coulomb stress modeling further, calculations were made on the Defne aftershock rupture due to both the February 6 Pazarcık and the largest aftershock earthquakes and the February 6 earthquake sequence. The stress models showed that the rupture of the Defne aftershock is located in the positive stress field for both cases (Fig. 4). When stress values were calculated for the Defne aftershock at different hypocentral locations, high positive stress values close to each other were obtained (Table 3). Accordingly, the stress values calculated at USGS, GCMT, AFAD and KOERİ hypocentral locations for the February 6 Pazarcık and the largest aftershock earthquakes are 0.234 bar, 2.009 bar, 1.912 bar and 1.097 bar, respectively, while the stress values obtained by taking into account the February 6 Elbistan earthquake are 0.116 bar, 2.121 bar, 1.878 bar and 1.107 bar, respectively. It is noteworthy that these high-stress values are almost the same as the stress values calculated only for the February 6 Pazarcık earthquake (Table 3). This suggests that the stress shadow created by the February 6 Elbistan earthquake had a negligible effect in delaying the rupture of the Defne aftershock and that the Defne aftershock rupture was predominantly triggered by the rupture of the February 6 Pazarcık earthquake. [6] and [103] emphasized that the Defne aftershock was triggered by the February 6 Pazarcık earthquake with a significant positive stress load in the epicenter region.

Table 3. The Coulomb stress change values calculated for different scenarios and locations.

		USGS (225/53/-27)			
		USGS	**GCMT**	**AFAD**	**KOERİ**
For Figures 3 and 4	**Long (°):**	36.025	36.06	36.037	36.10
	Lat (°):	36.162	36.03	36.021	36.13
	Calculation Depth (km):	11.5	12	21.73	16
		Coulomb stress changes (bar)			
	06 February Pazarcık Eq.	0.198	2.041	1.923	1.075
	Largest aftershock_6.7	0.005	0.002	0.002	0.004
	06 February Elbistan Eq.	-0.038	-0.029	-0.037	-0.038
	06 February Pazarcık+ Largest Aftershock	0.234	2.009	1.912	1.097
	06 February Pazarcık Eq. Largest Aftershock 06 February Elbistan Eq.	0.116	2.121	1.878	1.107
		Dead Sea Fault Plane (180/87/0)			
		P1	**P2**	**P3**	**P4**
For Figure 5	**Long (°):**	36.356	36.356	36.532	36.405
	Lat (°):	35.955	35.844	35.884	35.578
	Calculation Depth (km):	10			
		Coulomb stress changes (bar)			
	06 February Pazarcık Eq.	1.258	1.161	-0.306	0.486
	Largest aftershock_6.7	0.010	0.009	0.010	0.005
	06 February Elbistan Eq.	-0.001	-0.004	-0.018	-0.009
	Defne aftershock	0.060	-0.006	0.033	-0.015
	06 February Pazarcık Eq. Largest aftershock_6.7 06 February Elbistan Eq.	1.255	1.079	-0.279	0.448

In all stress models obtained in Fig. 5, the finite-fault slip distribution model we obtained for the rupture of the Defne aftershock was used. The Coulomb stress model calculated on the DSF due to the February 6 earthquake sequence, including the Defne aftershock, revealed that the northern part of the DSF is loaded with positive stress (Fig. 5a). This positive stress loading field indicates that the northern part of the DSF is more likely to rupture in the future. When the stress change model calculated only for the Defne aftershock in Fig. 5b is analyzed, it is noteworthy that the positive stress is negligibly small. Two major earthquakes occurred along the northern part of the DSF, one in the eastern segment in 1157 (M=7.0-7.5) and the other in the western segment in 1408 (M>7.5) [104]. The rupture zones of these earthquakes are shown in Fig. 5 (Transparent white areas). Points P1 and P2 are

selected on the 1408 earthquake rupture and points P3 and P4 are selected on the 1157 earthquake rupture. When Table 3 is examined, it is noteworthy that the 1408 fracture with high stress values (1.255 bar for the P1 point and 1.079 bar for the P2 point) is loaded with a triggering positive stress and the stress load is predominantly caused by the rupture of the February 6 Pazarcık earthquake. Although the rupture of the Defne aftershock created a stress load of 0.33 bar on point P3, it could not carry the stress shadow created by the February 6, earthquake to positive. Accordingly, point P3 is located in the stress shadow with a stress value of -0.279 bar. The stress load of 0.448 bar on point P4, located south of the 1157 rupture, is predominantly due to the rupture of the February 6 Pazarcık earthquake. The rupture of the Defne aftershock created a stress shadow of -0.015 bar at this point. On the other hand, the February 6 Elbistan earthquake created a stress shadow at all points, but this was not enough to delay a fault rupture. This is explained by the location of the February 6 Elbistan earthquake rupture and the distance from the points where stress calculations were performed. The absence of a large-scale earthquake north of the DSF for more than 600 years, the positive Coulomb stress changes values caused predominantly by the February 6 Pazarcık earthquake, and the negligible effect of the Defne aftershock rupture have increased the probability of future rupture in this part of the fault, perhaps bringing it forward. Therefore, special attention should be paid to this fault.

5. Conclusions

Here, a finite-fault slip distribution model was obtained from the inversion of the teleseismic P waveforms of the February 20, 2023, Defne aftershock, which occurred shortly after the devastating February 6 Pazarcık and Elbistan earthquakes. The slip model showed that the rupture was caused by the rupture of an asperity located between 6-12 km depth with a maximum displacement of about 0.75 m. The rupture propagated unilaterally from the hypocenter to the NE. A total seismic moment of 5.85×10^{18} Nt.m was released. Coulomb stress change modeling showed that the high positive stress load from the rupture of the February 6 Pazarcık earthquake played the dominant triggering role in the rupture of the Defne aftershock. In addition, stress variation modeling on the DSF showed high positive stress values in the northern part. The positive stress load and the fact that no major earthquake has occurred for a long time showed that the seismic risk for the northern part of the DSF is high.

Author Contribution

The writing of the manuscript and all analyses were performed by Hatice Durmuş.

Acknowledgements

I thank Dr Murat UTKUCU for his contributions to the manuscript. Some figures were generated using the [105].

References

[1] Afet ve Acil durum Yönetimi Deprem Dairesi Başkanlığı, "06 Şubat 2023 Pazarcık-Elbistan Kahramanmaraş (Mw:7.7-Mw:7.6) Depremleri Raporu", [Online] https://deprem.afad.gov.tr/assets/pdf/Kahramanmara%C5%9F%20Depremi%20%20Raporu_02.06.2023.pdf [Access date: 05 February 2024]

[2] T.C. Cumhurbaşkanlığı Strateji ve Bütçe Başkanlığı, "Kahramanmaraş ve Hatay Depremleri Raporu", [Online] https://www.sbb.gov.tr/2023-kahramanmaras-ve-hatay-depremleri-raporu/ [Access date: 15 February 2024]

[3] World Healty Organization, "Emergency situation report", https://www.who.int/europe/emergencies/situations/turkiye-and-syria-earthquakes/situation-reports, [Access date: 25 January 2024]

[4] F. Şaroğlu, O. Emre, I. Kuscu, "Active fault map of Turkey", General Directorate of Mineral Research and Exploration, [Access date: 25 January 2024]

[5] T. Y. Duman and Ö. Emre, "The East Anatolian Fault: geometry, segmentation and jog characteristics", *Geological Society, London, Special Publications*, 372.1: 495-529, 2013, doi.org/10.1144/SP372.14.

[6] J.J. Zhao, Q. Chen, Y.H. Yang, & Q. Xu, "Coseismic faulting model and post-seismic surface motion of the 2023 Turkey–Syria earthquake doublet revealed by InSAR and GPS measurements," *Remote Sensing*, 15.13: 3327, 2023, doi.org/10.3390/rs15133327.

[7] A. A. Barka and K. Kadinsky- Cade, "Strike- slip fault geometry in Turkey and its influence on earthquake activity," *Tectonics*, 7.3: 663-684, 1988, doi.org/10.1029/TC007i003p00663.
[8] N. N. Ambraseys, "Temporary seismic quiescence: SE Turkey," *Geophysical Journal International*, 96.2: 311-331, 1989, doi.org/10.1111/j.1365-246X.1989.tb04453.x.
[9] T. Taymaz, H. Eyidoğan, & J. Jackson, Source parameters of large earthquakes in the East Anatolian Fault Zone (Turkey). *Geop J. Int.*, *106*(3), 537-550, 1991.
[10] Ö. Emre, T. Y. Duman, S. Özalp, H. Elmacı, Ş. Olgun, & F. Şaroğlu, "Active fault map of Turkey with explanatory text". *General directorate of mineral research and exploration special publication series*, *30*, *2013*.
[11] O. Tan, Z. Pabuçcu, M. C. Tapırdamaz, S. İnan, S. Ergintav, H. Eyidoğan,... & F. Kuluöztürk, "Aftershock study and seismotectonic implications of the 8 March 2010 Kovancılar (Elazığ, Turkey) earthquake (MW= 6.1)", *Geophysical Research Letters*, *38*(11), 2011.
[12] M. Utkucu, E. Budakoğlu & M. Çabuk, "Teleseismic finite-fault inversion of two M w= 6.4 earthquakes along the East Anatolian Fault Zone in Turkey: the 1998 Adana and 2003 Bingöl earthquakes". *Arabian Journal of Geosciences*, *11*, 1-14, 2018.
[13] M. Utkucu, "Türkiye'de Zaman Bağımlı Deprem Gerilme Etkileşimlerinin Modellenmesi ve Deprem Tehlikesi Üzerine Çıkarımlar" *TÜBİTAK Proje No: 121Y271*, *2023*.
[14] A. Hubert-Ferrari, L. Lamair, S. Hage, S. Schmidt, M.N. Çağatay, & U. Avşar, "A 3800 yr paleoseismic record (Lake Hazar sediments, eastern Turkey): Implications for the East Anatolian Fault seismic cycle," *Earth and Planetary Science Letters*, 538: 116152, 2020, doi.org/10.1016/j.epsl.2020.116152.
[15] S. Mcclusky, S. Balassanian, A. Barka, C. Demir, S. Ergintav, I. Georgiev & G. Veis, "Global Positioning System constraints on plate kinematics and dynamics in the eastern Mediterranean and Caucasus," *Journal of Geophysical Research: Solid Earth*, 105.B3: 5695-5719, 2000, doi.org/10.1029/1999JB900351.
[16] R. Reilinger, S. McClusky, P. Vernant, S. Lawrence, S. Ergintav, R. Cakmak & G. Karam, "GPS constraints on continental deformation in the Africa- Arabia- Eurasia continental collision zone and implications for the dynamics of plate interactions," *Journal of Geophysical Research: Solid Earth*, 111.B5, 2006, doi:10.1029/2005JB004051.
[17] A. Hubert-Ferrari, G. King, I. Manighetti, R. Armijo, B. Meyer, & P. Tapponnier, "Long-term elasticity in the continental lithosphere; modelling the Aden Ridge propagation and the Anatolian extrusion process," *Geophysical Journal International*, 153.1: 111-132, 2003, doi.org/10.1046/j.1365-246X.2003.01872.x.
[18] O. Tatar, J.D.A. Piper, H. Gürsoy, A. Heimann, & F. Koçbulut, "Neotectonic deformation in the transition zone between the Dead Sea Transform and the East Anatolian Fault Zone, Southern Turkey: a palaeomagnetic study of the Karasu Rift Volcanism," *Tectonophysics*, 385.1-4: 17-43, 2004, doi.org/10.1016/j.tecto.2004.04.005
[19] A.M.C. Şengör, O. Tüysüz, C. Imren, M. Sakınç, H. Eyidoğan, N. Görür,... & C. Rangin, "The North Anatolian fault: A new look," *Annu. Rev. Earth Planet. Sci.*, 33: 37-112, 2005, doi.org/10.1146/annurev.earth.32.101802.120415.
[20] N. N. Ambraseys, "Some characteristic features of the Anatolian fault zone," *Tectonophysics*, 9.2-3: 143-165, 1970, doi.org/10.1016/0040-1951(70)90014-4.
[21] R. Armijo, B. Meyer, A. Hubert, & A. Barka, "Westward propagation of the North Anatolian fault into the northern Aegean: Timing and kinematics," *Geology*, 27.3: 267-270, 1999, doi.org/10.1130/0091-7613(1999)027<0267:WPOTNA>2.3.CO;2
[22] A. Hubert‐Ferrari, R. Armijo, G. King, B. Meyer, & A. Barka, "Morphology, displacement, and slip rates along the North Anatolian Fault, Turkey," *Journal of Geophysical Research: Solid Earth*, 107.B10: ETG 9-1-ETG 9-33, 2002.
[23] X. Le Pichon, A.C. Şengör, J. Kende, C. İmren, P. Henry, C. Grall, H. & Karabulut, "Propagation of a strike-slip plate boundary within an extensional environment: the westward propagation of the North Anatolian Fault," *Canadian Journal of Earth Sciences*, 53.11: 1416-1439, 2016, doi.org/10.1139/cjes-2015-0129.
[24] M. Cengiz, S. Karabulut, "A two-stage deformation of the Anatolian Plate deduced from Paleomagnetic signals: The initial age of the Anatolian's escape". *Turkish Journal of Earth Sciences*, *33*(3), 243-259, 2024.
[25] B. Aktug, H. Ozener, A. Dogru, A. Sabuncu, B. Turgut, K. Halicioglu,... & E. Havazli, "Slip rates and seismic potential on the East Anatolian Fault System using an improved GPS velocity field," *Journal of Geodynamics*, 94: 1-12, 2016, doi.org/10.1016/j.jog.2016.01.001.
[26] R. Westaway, "Kinematic consistency between the Dead Sea Fault Zone and the Neogene and Quaternary left-lateral faulting in SE Turkey". *Tectonophysics*, *391*(1-4), 2004, 203-237.
[27] A. Seyrek, T. Demir, R. Westaway, H. Guillou, S. Scaillet, T. S. White, & D. R. Bridgland, "The kinematics of central-southern Turkey and northwest Syria revisited". *Tectonophysics*, 2014, *618*, 35-66.
[28] E. Altunel, M. Meghraoui, V. Karabacak, S. H. Akyüz, M. Ferry, Ç. Yalçıner, & M. Munschy, "Archaeological sites (tell and road) offset by the dead sea fault in the Amik Basin, southern Turkey". *Geophysical Journal International*, *179*(3), 1313-1329, 2009.
[29] Y. Mahmoud, F. Masson, M. Meghraoui, Z. Cakir, A. Alchalbi, H. Yavasoglu, & S. Inan, "Kinematic study at the junction of the East Anatolian fault and the Dead Sea fault from GPS measurements". *Journal of Geodynamics*, *67*, 30-39, 2013.
[30] E. Herece "Atlas of the East Anatolian Fault (1:500,000)". General Directorate of Mineral Research and Exploration of Turkey (MTA), Ankara, Turkey. Special Publication Series 13:13,359, 2008.
[31] R.D. Hartleb, J.F. Dolan, H.S. Akyüz, & B. Yerli, "A 2000-year-long paleoseismologic record of earthquakes along the central North Anatolian Fault, from trenches at Alayurt, Turkey," *Bulletin of the Seismological Society of America*, 93.5: 1935-1954, 2003, doi.org/10.1785/0120010271.
[32] M. Bohnhoff, P. Martínez-Garzón, F. Bulut, E. Stierle, & Y. Ben-Zion, "Maximum earthquake magnitudes along different sections of the North Anatolian fault zone," *Tectonophysics*, 674: 147-165, 2016, doi.org/10.1016/j.tecto.2016.02.028.
[33] B. Willis, "Dead Sea problem: rift valley or ramp valley?", *Bulletin of the Geological Society of America*, *39*(2), 490-542, 1928.

[34], K. Ergin "A catalogue of earthquakes for Turkey and surrounding area (11AD to 1964AD)". *Tech. Univ. Mining Eng. Fac. Publ.*, *24*, 189, 1967.
[35] J. P. Poirier, & M. A. Taher, "Historical seismicity in the near and Middle East, North Africa, and Spain from Arabic documents (VIIth-XVIIIth century)". *Bulletin of the Seismological Society of America*, *70*(6), 2185-2201, 1980.
[36] H. Soysal, S. Sipahioğlu, D. Kolçak, & Y. Altınok, Türkiye ve çevresinin tarihsel deprem kataloğu. *TÜBİTAK Proje No: TBAG*, *341*, 124, (1981).
[37] N. N. Ambraseys, & J. A. Jackson, "Faulting associated with historical and recent earthquakes in the Eastern Mediterranean region". *Geophysical Journal International*, *133*(2), 390-406, 1998.
[38] S.S. Nalbant, J. McCloskey, S. Steacy, & A.A. Barka, "Stress accumulation and increased seismic risk in eastern Turkey," *Earth and Planetary Science Letters*, 195.3-4: 291-298, 2002, doi.org/10.1016/S0012-821X(01)00592-1.
[39] Ö. Yönlü, & V. Karabacak, "Surface rupture history and 18 kyr long slip rate along the Pazarcık segment of the East Anatolian Fault". *Journal of the Geological Society*, *181*(1), jgs2023-056, 2024.
[40] R. E. Tatevossian, N. G. Mokrushina, A. N. Ovsyuchenko, & A. S. Larkov, "Historical Earthquake on the North-Eastern Extension of the East Anatolian Fault". *Izvestiya, Physics of the Solid Earth*, *59*(6), 878-887, 2023.
[41] H. Karabulut, S. E. Güvercin, J. Hollingsworth, & A. Ö. Konca, "Long silence on the East Anatolian Fault Zone (Southern Turkey) ends with devastating double earthquakes (6 February 2023) over a seismic gap: implications for the seismic potential in the Eastern Mediterranean region". *Journal of the Geological Society*, *180*(3), jgs2023-021, 2023.
[42] H. Alkan, A. Büyüksaraç, & Ö. Bektaş, "Investigation of earthquake sequence and stress transfer in the Eastern Anatolia Fault Zone by Coulomb stress analysis". Turkish Journal of Earth Sciences, 33(1), 56-68, 2024.
[43] R.E. Tatevossian, N.G. Mokrushina, A.N. Ovsyuchenko, & A.S. Larkov, "Historical Earthquake on the North-Eastern Extension of the East Anatolian Fault". *Izvestiya, Physics of the Solid Earth*, *59*(6), 878-887, 2023.
[44] Ö. Yönlü, V. Karabacak, E. Altunel, H.S. Akyüz, "Paleoseismological slip rate on the East Anatolian fault zone around Türkoğlu," *International Earth Science Colloquium on the Aegean Region, IESCA-2012*, 2012, p. 1-5.
[45] Yönlü, Ö. (2012). Doğu Anadolu Fay Zonunun Gölbaşı (Adıyaman) İle Karataş (Adana) arasındaki kesiminin geç kuvaterner aktivitesi.
[46] S. Li, X. Wang, T. Tao, Y. Zhu, X. Qu, Z. Li, & S. Song, "Source Model of the 2023 Turkey Earthquake Sequence Imaged by Sentinel-1 and GPS Measurements: Implications for Heterogeneous Fault Behavior along the East Anatolian Fault Zone," *Remote Sensing*, 15.10: 2618, 2023, doi.org/10.3390/rs15102618.
[47] AFAD (Şubat 2023). 06 Şubat 2023 Kahramanmaraş (Pazarcık ve Elbistan) Depremleri Saha Çalışmaları Ön Değerlendirme Raporu, Deprem Dairesi Başkanlığı, Available:https://deprem.afad.gov.tr/assets/pdf/Arazi_Onrapor_28022023_surum1_revize.pdf
[48] S. Barbot, H. Luo, T. Wang, Y. Hamiel, O. Piatibratova, M.T. Javed,... & G. Gurbuz, "Slip distribution of the February 6, 2023 Mw 7.8 and Mw 7.6, Kahramanmaraş, Turkey earthquake sequence in the East Anatolian fault zone," *Seismica*, ISSN 2816-9387 volume 2.3, 2023, *doi.org/10.26443/seismica.v2i3.502*.
[49] D. Melgar, T. Taymaz, A. Ganas, B.W. Crowell, T. Öcalan, M. Kahraman,... & C. Altuntaş, "Sub-and super-shear ruptures during the 2023 Mw 7.8 and Mw 7.6 earthquake doublet in SE Türkiye," *Seismica*, vol. 2.3, 2023, doi.org/10.26443/seismica.v2i3.387.
[50] C. Liu, T. Lay, R. Wang, T. Taymaz, Z. Xie, X. Xiong, & C. Erman, "Complex multi-fault rupture and triggering during the 2023 earthquake doublet in southeastern Türkiye," *Nature Communications*, 14:5564, 2023, doi.org/10.1038/s41467-023-41404-5
[51] J.R. Elliott, E.K. Nissen, P.C. England, J.A. Jackson, S. Lamb, Z. Li, & B. Parsons, "Slip in the 2010–2011 Canterbury earthquakes, New Zealand," *Journal of Geophysical Research: Solid Earth*, 117.B3, 2012, doi.org/10.1029/2011JB008868.
[52] M. Utkucu, "23 October 2011 Van, Eastern Anatolia, earthquake (M_W 7.1) and seismotectonics of Lake Van area," *Journal of seismology*, 17: 783-805, 2013, doi.org/10.1007/s10950-012-9354-z.
[53] M. Utkucu, H. Durmuş, H. Yalçın, E. Budakoğlu, & E. Işık, "Coulomb static stress changes before and after the 23 October 2011 Van, eastern Turkey, earthquake (M W= 7.1): implications for the earthquake hazard mitigation," *Natural Hazards and Earth System Sciences*, 13.7: 1889-1902, 2013, doi.org/10.5194/nhess-13-1889-2013.
[54] R.S. Stein, "Earthquake conversations," *Scientific American*, January 2003, 288.1: 72-79.
[55] A.M. Freed, "Earthquake triggering by static, dynamic, and postseismic stress transfer," *Annu. Rev. Earth Planet. Sci.*, 33: 335-367, 2005, doi.org/10.1146/annurev.earth.33.092203.122505.
[56] R.A. Harris and R.W. Simpson, "Changes in static stress on southern California faults after the 1992 Landers earthquake," *Nature*, 360.6401: 251-254, 1992, doi.org/10.1038/360251a0.
[57] R.S. Stein, G.C.P. King, J. Lin, "Change in failure stress on the southern San Andreas fault system caused by the 1992 magnitude= 7.4 Landers earthquake," *Science*, 258.5086: 1328-1332, 1992, doi: 10.1126/science.258.5086.1328.
[58] R.S. Stein, G.C.P, King, J. Lin, "Stress triggering of the 1994 M= 6.7 Northridge, California, earthquake by its predecessors," *Science*, 265.5177: 1432-1435, 1994, doi: 10.1126/science.265.5177.14.
[59] R.S. Stein, A.A. Barka, J.H. Dieterich, "Progressive failure on the North Anatolian fault since 1939 by earthquake stress triggering," *Geophysical Journal International*, 128.3: 594-604, 1997, doi.org/10.1111/j.1365-246X.1997.tb05321.x.
[60] G.C.P. King, R.S. Stein, J. Lin, "Static stress changes and the triggering of earthquakes," *Bulletin of the Seismological Society of America*, 84.3: 935-953, 1994, doi.org/10.1785/BSSA0840030935.
[61] G.C.P. King, "Fault interaction, earthquake stress changes, and the evolution of seismicity," *Earthquake Seismology*, 4: 225-255, 2007, doi. org/ 10. 1016/ B978- 04445 2748-6. 00069-9.
[62] A. Hubert, G. King, R. Armijo, B. Meyer, & D. Papanastasiou, "Fault re-activation, stress interaction and rupture propagation of the 1981 Corinth earthquake sequence," *Earth and Planetary Science Letters*, 142.3-4: 573-585, 1996, doi.org/10.1016/0012-821X(96)00108-2.
[63] R.A. Harris, "Introduction to special section: Stress triggers, stress shadows, and implications for seismic hazard," *Journal of Geophysical*

Res: Solid Earth, 103.B10:24347-24358, 1998, doi.org/10.1029/98JB01576.
[64] S.S. Nalbant, A. Hubert, G.C.P. King, "Stress coupling between earthquakes in northwest Turkey and the north Aegean Sea," *Journal of Geophysical Research: Solid Earth*, 103.B10: 24469-24486, 1998, doi.org/10.1029/98JB01491.
[65] S. Toda, R.S. Stein, P.A. Reasenberg, J.H. Dieterich, & A. Yoshida, "Stress transferred by the 1995 Mw= 6.9 Kobe, Japan, shock: Effect on aftershocks and future earthquake probabilities," *Journal of Geophysical Research: Solid Earth*, 103.B10: 24543-24565, 1998, doi.org/10.1029/98JB00765
[66] A. Hubert-Ferrari, A. Barka, E. Jacques, S.S. Nalbant, B. Meyer, R. Armijo & G.C. King, "Seismic hazard in the Marmara Sea region following the 17 August 1999 Izmit earthquake," *Nature*, March 2000, 404.6775: 269-273.
[67] F. Pollitz, M. Vergnolle, E. Calais, "Fault interaction and stress triggering of twentieth century earthquakes in Mongolia," *Journal of Geophysical Research: Solid Earth*, 108.B10, 2003, doi.org/10.1029/2002JB002375.
[68] J. Lin and R.S. Stein, "Stress triggering in thrust and subduction earthquakes and stress interaction between the southern San Andreas and nearby thrust and strike- slip faults," *Journal of Geophysical Research: Solid Earth*, 109.B2, 2004, doi.org/10.1029/2003JB002607.
[69] T. Parsons and D.S. Dreger, "Static- stress impact of the 1992 Landers earthquake sequence on nucleation and slip at the site of the 1999 M= 7.1 Hector Mine earthquake, southern California," G*eophysical research letters*, 27.13: 1949-1952, 2000, doi.org/10.1029/1999GL011272
[70] M. Wyss and S. Wiemer, "Change in the probability for earthquakes in southern California due to the Landers magnitude 7.3 earthquake," *Science*, 290.5495: 1334-1338, 2000, doi: 10.1126/science.290.5495.13.
[71] H. Durmuş, "İran depremlerinin faylanma özelliklerinin ve deprem gerilme etkileşimlerinin modellenmesi." Doktora Tezi, Sakarya Üniversitesi Fen Bilimleri Enstitüsü, 2014.
[72] M. Utkucu, H. Durmuş, S. Nalbant, "Stress history controls the spatial pattern of aftershocks: case studies from strike-slip earthquakes," *International Journal of Earth Sciences*, 106: 1841-1861, 2017, doi.org/10.1007/s00531-016-1389-x.
[73] S.H. Hartzell and T.H. Heaton, "Inversion of strong ground motion and teleseismic waveform data for the fault rupture history of the 1979 Imperial Valley, California, earthquake," *Bulletin of the Seismological Society of America*, 73.6A: 1553-1583, 1983, doi.org/10.1785/BSSA07306A1553.
[74] S.H. Hartzell, G.S. Stewart, C. Mendoza, "Comparison of L 1 and L 2 norms in a teleseismic waveform inversion for the slip history of the Loma Prieta, California, earthquake," *Bulletin of the Seismological Society of America*, 81.5: 1518-1539, 1991, doi.org/10.1785/BSSA0810051518.
[75] D.J. Wald, D.V. Helmberger, T.H. Heaton, "Rupture model of the 1989 Loma Prieta earthquake from the inversion of strong-motion and broadband teleseismic data," *Bulletin of the Seismological Society of America*, 81.5: 1540-1572, 1991, doi.org/10.1785/BSSA0810051540.
[76] D.J. Wald and T.H. Heaton, "Spatial and temporal distribution of slip for the 1992 Landers, California, earthquake," *Bulletin of the Seismological Society of America*, 84.3: 668-691, 1994, doi.org/10.1785/BSSA0840030668.
[77] C. Mendoza, "Coseismic slip of two large Mexican earthquakes from teleseismic body waveforms: Implications for asperity interaction in the Michoacan plate boundary segment," *Journal of Geophysical Research: Solid Earth*, 98.B5: 8197-8210, 1993, doi.org/10.1029/93JB00021.
[78] C. Mendoza, "Finite-fault analysis of the 1979 March 14 Petatlan, Mexico, earthquake using teleseismic P waveforms," *Geophysical Journal International*, 121.3: 675-683, 1995.
[79] M. Utkucu, *et al*. "Slip distribution and stress changes associated with the 1999 November 12, Düzce (Turkey) earthquake (Mw= 7.1)," *Geophysical Journal International*, 153.1: 229-241, 2003.
[80] C.A. Langston and D.V. Helmberger, "A procedure for modelling shallow dislocation sources," *Geophysical Journal International*, 42.1: 117-130, 1975, doi.org/10.1111/j.1365-246X.1975.tb05854.x.
[81] C. Mendoza, & S.H. Hartzell, 1988. Inversion for slip distribution using teleseismic Pwaveforms: North Palm Springs, Borah Peak and Michoacan earthquakes, *Bull. seism. Soc. Am.*, 78, 1092–1111.
[82] W. Menke, "Geophysical Data Analysis: Discrete Inverse Theory," International Geophysics Series, Vol. 45, Academic Press, Inc., San Diego, California 92101, ISBN -0-12-490921-3, 1989.
[83] S.S. Nalbant, A.A. Barka, Ö. Alptekin, "Failure stress change caused by the 1992 Erzincan earthquake (Ms= 6.8)," *Geophysical research letters*, 23.13: 1561-1564, 1996, doi.org/10.1029/96GL01323.
[84] R. S. Stein, "The role of stress transfer in earthquake occurrence," *Nature*, 402.6762: 605-609, 1999, doi.org/10.1038/45144.
[85] S. Toda and R.S. Stein, "Toggling of seismicity by the 1997 Kagoshima earthquake couplet: a demonstration of time-dependent stress transfer," *Journal of Geophysical Res.: Solid Earth*, 108. B12, 2003, doi.org/10.1U029/2003JB002527
[86] O. Heidbach and Z. Ben-Avraham, "Stress evolution and seismic hazard of the Dead Sea fault system," *Earth and Planetary Science Letters*, 257.1-2: 299-312, 2007, doi.org/10.1016/j.epsl.2007.02.042.
[87] X. Liu, Q. Chen, Y. Yang, Q. Xu, J. Zhao, L. Xu, & R. Liu, "The 2021 Mw7. 4 Maduo earthquake: Coseismic slip model, triggering effect of historical earthquakes and implications for adjacent fault rupture potential," *Journal of Geodynamics*, 151: 101920, 2022, doi.org/10.1016/j.jog.2022.101920.
[88] M. Utkucu, F. Uzunca, H. Durmuş, S.S. Nalbant, C. İpek, & Ş. Ramazanoğlu, "The M w= 5.8 2019 Silivri earthquake, NW Türkiye: is it a warning beacon for a big one?," *International Journal of Earth Sciences*, 2024, 113.1: 107-124.
[89] C. Liu, P. Dong, Y. Shi, "Stress change from the 2015 Mw 7.8 Gorkha earthquake and increased hazard in the southern Tibetan Plateau," *Physics of the Earth and Planetary Interiors*, 267: 1-8, 2017, doi.org/10.1016/j.pepi.2017.04.002.
[90] W.D. Barnhart, G.P. Hayes, R.D. Gold, "The July 2019 Ridgecrest, California, earthquake sequence: Kinematics of slip and stressing in cross- fault ruptures," *Geophysical Research Letters*, 46.21: 11859-11867, 2019, doi.org/10.1029/2019GL084741
[91] S. Li, G. Chen, T. Tao, P. He, K. Ding, R. Zou,... & Q. Wang, "The 2019 M w 6.4 and M w 7.1 Ridgecrest earthquake sequence in eastern California: Rupture on a conjugate fault structure revealed by GPS and InSAR measurements," *Geophysical Journal International*, 221.3: 1651-1666, 2020, doi.org/10.1093/gji/ggaa099.

[92] D.E. Goldberg, D. Melgar, V.J. Sahakian, A.M. Thomas, X. Xu, B.W. Crowell, & J Geng, "Complex rupture of an immature fault zone: A simultaneous kinematic model of the 2019 Ridgecrest, CA earthquakes," *Geophysical Research Letters*, 47.3, 2020, doi.org/10.1029/2019GL086382.
[93] S. Steacy, J. Gomberg, M. Cocco, "Introduction to special section: Stress transfer, earthquake triggering, and time- dependent seismic hazard," *Journal of Geophysical Research: Solid Earth*, 110.B5, 2005, doi.org/10.1029/2005JB003692.
[94] P.S. Raju, V.K. Gahalaut, K.M. Ravi, "Phodong (Sikkim) earthquake of 14 February 2006 and its aftershocks-Coulomb stress analysis," *Journal of Geodynamics*, 46.1-2: 63-67, 2008, doi.org/10.1016/j.jog.2008.04.001.
[95] S. Lasocki, V.G. Karakostas, E.E. Papadimitriou, "Assessing the role of stress transfer on aftershock locations," *Journal of Geophysical Research: Solid Earth*, 114.B11, 2009, doi.org/ 10.1029/2008JB006022.
[96] T. Sato, S. Hiratsuka, J. Mori, "Coulomb stress change for the normal-fault aftershocks triggered near the Japan Trench by the 2011 M w 9.0 Tohoku-Oki earthquake," *Earth, planets and space*, 64: 1239-1243, 2012, doi.org/10.5047/eps.2012.04.003.
[97] M. Cocco, C. Nostro, G. Ekström, "Static stress changes and fault interaction during the 1997 Umbria-Marche earthquake sequence," *Journal of Seismology*, 4: 501-516, 2000, doi.org/10.1023/A:1026507917308.
[98] S. Steacy, D. Marsan, S.S. Nalbant, & J. McCloskey, "Sensitivity of static stress calculations to the earthquake slip distribution," J*ournal of Geophysical Research: Solid Earth*, 2004, 109.B4, doi.org/10.1029/2002JB002365.
[99] Y. Okada, "Internal deformation due to shear and tensile faults in a half-space," *Bulletin of the seismological society of America*, 82.2: 1018-1040, 1992, doi.org/10.1785/BSSA0820021018.
[100] S. Toda, R.S. Stein, K.R. Dinger, S. Bozkurt, "Forecasting the evolution of seismicity in southern California: Animations built on earthquake stress transfer," *Journal of Geophysical Research: Solid Earth*, 110.B5, 2005, doi.org/10.1029/2004JB003415
[101] D.L. Wells and K.J. Coppersmith, "New empirical relationships among magnitude, rupture length, rupture width, rupture area, and surface displacement," *Bulletin of the seismological Society of America*, 84.4: 974-1002, 1994, https://doi.org/10.1785/BSSA0840040974
[102] Ö., Emre, T. Y., Duman, S., Özalp, F., Şaroğlu, Ş., Olgun, H., Elmacı, & T. Çan, "Active fault database of Turkey," *Bulletin of Earthquake Engineering*, 16.8: 3229-3275, 2018, doi.org/10.1007/s10518-016-0041-2.
[103] M. Utkucu, F. Uzunca, H. Durmuş, S. Nalbant, & S. Sert, "The 2023 Pazarcık (Mw=7.8) and Elbistan (Mw=7.6), Kahramanmaraş Earthquakes in the southeast, Türkiye", [Online], http://www.aym.sakarya.edu.tr/2023/02/24/the-2023-pazarcik-mw7-8-and-elbistan-mw7-6-kahramanmaras-earthquakes-in-the-southeast-turkiye/ 22 February 2023, [Access date: 25 January 2024].
[104] M. Meghraoui, F. Gomez, R. Sbeinati, J. Van der Woerd, M. Mouty, A.N. Darkal, & M. Barazangi, "Evidence for 830 years of seismic quiescence from palaeoseismology, archaeoseismology and historical seismicity along the Dead Sea fault in Syria," *Earth and Planetary Science Letters*, 210.1-2: 35-52, 2003, doi.org/10.1016/S0012-821X(03)00144-4.
[105] P. Wessel and W.H.F. Smith, "New, improved version of Generic Mapping Tools released," *Eos, Transactions American Geophysical Union*, 79.47: 579-579, 1998, doi.org/10.1029/98EO00426.